applied sciences

MDPI

Article

Numerical and Analytical Analysis of the Low-Frequency Magnetic Fields Generated by Three-Phase Underground Power Cables with Solid Bonding

Eduard Lunca *, Silviu Vornicu and Alexandru Sălceanu

Department of Electrical Measurements and Materials, "Gheorghe Asachi" Technical University of Iasi, 23 Professor Dimitrie Mangeron Blvd., 700050 Iasi, Romania; silviu-constantin.vornicu@academic.tuiasi.ro (S.V.); asalcean@tuiasi.ro (A.S.)
* Correspondence: elunca@tuiasi.ro; Tel.: +40-232-701246

Abstract: There is a special concern for measuring and simulating low-frequency magnetic fields generated by underground power cables, particularly in human exposure studies. In the present study, an accurate 2D finite element model for computing magnetic fields generated by three-phase underground power cables with solid bonding is proposed. The model is developed in ANSYS Maxwell 2D low-frequency electromagnetic field simulation software for a typical 12/20 kV (medium-voltage) three-phase underground power cable in both trefoil and flat formations, but it can be adapted to any cable system. Model validation is achieved by analytical computations conducted with a software tool based on the Biot–Savart law and the superposition principle. RMS magnetic flux density profiles calculated at various heights above the ground with these two methods correlate very well. This is also true for induced shield currents. The application of the finite element model to multiple three-phase power cables laid together is also considered.

Keywords: magnetic field; underground power cable; solid bonding; finite element model; analytical calculation

Citation: Lunca, E.; Vornicu, S.; Sălceanu, A. Numerical and Analytical Analysis of the Low-Frequency Magnetic Fields Generated by Three-Phase Underground Power Cables with Solid Bonding. *Appl. Sci.* **2023**, *13*, 6328. https://doi.org/10.3390/app13106328

Academic Editor: Mario Lucido

Received: 21 April 2023
Revised: 16 May 2023
Accepted: 19 May 2023
Published: 22 May 2023

1. Introduction

The general concern and implicit interest in monitoring the low-frequency magnetic fields generated by underground electric cables (in either transmission or especially distribution networks) has recently been augmented. If in the case of the high-voltage transmission systems, underground power cables are a solution only in certain special cases (water or wide road crossings or particularly scenic areas), we can say that in the urban distribution area, underground power cables (of medium voltage) are an increasingly applied solution. Assembly and installation costs are considerably higher by comparison with the overhead solution, but aesthetics and reliability are significantly improved, leading to reductions of up to 10 fold in outage duration. On the other hand, the three-phase underground power cables in the distribution systems, which may carry currents of hundreds of amperes at voltages of tens or sometimes even hundreds of kV, are found in the immediate vicinity of humans, much closer than overhead power lines. What are the values of the electric and magnetic fields generated and to what extent can they be controlled and reduced is a question that concerns every citizen. Consequently, the specialists must provide scientifically based answers [1].

Regarding electric fields, the shielding effect achieved due to the Faraday cage principle is very strong, being mainly produced by the conductive metallic screen/shield that protects any underground cable (when bonded to ground, it will also carry out the short circuit fault current), or by the ground in which the cable is buried (which has some conductive properties). In contrast, shielding magnetic fields is much more complicated and expensive. There are two techniques: ferromagnetic shielding (performed with shields made of materials with high magnetic permeability, on the principle of the path of minimum reluctance) and induced current shielding (which is effective only if the shield is a good electrical conductor and thick enough). In addition to high costs and constructive-technological difficulties, these solutions for shielding magnetic fields also have the important disadvantage of increasing the losses produced by line charging currents. That is why they will be applied only on relatively short distances and only in the case of very special requirements [2,3].

Therefore, as in the case of overhead power lines, it is strongly recommended that through analytical calculations, numerical modeling or actual measurements, to be verified that the low-frequency magnetic field generated by underground power cables at the soil level is (far) below the values considered acceptable by the health regulations. Computations, which can be quite accurate, are often preferable to measurements because they can be performed for any desired scenario, rather than being limited to the particular conditions at the measurement time [4–8].

A common 2D approach for calculating magnetic fields generated by underground power cables is based on the Biot–Savart law and the superposition principle, assuming that the cables are straight, horizontal, infinitely long and parallel to each other and the effect of the induced shield currents on the magnetic field is negligible [9–12]. Basically, this is the case for single-point bonding systems and cross-bonding systems, in which the induced shield currents are zero or insignificant. However, when dealing with solid bonding (i.e., the underground power cables operate with their metallic shields bonded and grounded at both ends), the circulating currents induced in shields may achieve the same order as the wire-core currents, which leads to a certain total magnetic field reduction. In some studies, e.g., [13,14], analytical expressions for the induced shield currents have been obtained under balanced three-phase conditions. It has also been considered the magnetic field reduction.

Some 2D finite element method (FEM) models have also been developed for computing magnetic fields from three-phase underground cables with solid bonding. In [15], COMSOL Multiphysics is used to investigate the magnetic field reduction rate for a three-phase cable in flat formation as a function of the distance between cables, the shield diameter, as well as the cross-sectional area of the cable shields. In [16], QuickField was mainly used for predicting underground cable ampacity (for both trefoil and flat formations), while the developed model also allows investigating the magnetic field distribution at the ground surface (only limited results are presented). For a similar purpose (flat formation only), ANSYS Maxwell is used in [17].

In our study, which is an extended version of [18], FEM based on ANSYS Maxwell (2D) software is used to compute low-frequency magnetic fields generated by three-phase underground power cables with solid bonding according to the usual procedures applied in human exposure studies. Both trefoil and flat formations of a 12/20 kV (medium-voltage) three-phase power cable are considered for FEM model implementation. For its validation, calculated magnetic fields and induced shield currents are checked by comparison with analytical results obtained with a software tool based on the Biot–Savart law and the superposition principle, which represents an updated version of a previously developed program [19]. Finally, the application of the FEM model to multiple three-phase power cables laid together is considered. In all cases, the magnetic field reduction rate due to induced shield currents is determined as well.

The computational time, generally a major drawback of using FEM [20], is, in this study, quite acceptable, in the order of 10 to 25 min (simple cable formation, depending on mesh size). Compared to the analytical approach, which is limited to simple trefoil and flat formations of cables, the FEM model can also be applied to various types of cable arrangements while taking into account different influencing factors, such as the relative phase sequences and positions of the cables. Hence, it may be used not only for assessing compliance with relevant magnetic field exposure regulations, but also as an accurate tool for optimizing cable layout and location to mitigate magnetic field problems. Usually, the modification of the total magnetic field due to induced shield currents is not considered in the commercially available software for power cable system analysis.

2. Physical Model Selected for Analysis

The single-core power cables in a three-phase circuit can be laid out in a number of formations. Typical ones are trefoil and flat. In the first case, the three cables are placed in the corners of an equilateral triangle, as presented in Figure 1a; in the second case, the three cables are placed in the same horizontal plane, at equal distances between adjacent cables, as presented in Figure 1b. The choice of use depends on several factors such as shield bonding method, conductor area and available space for installation [21,22].

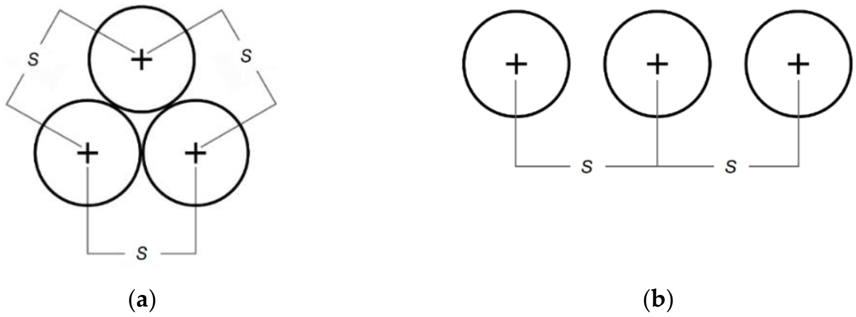

Figure 1. Typical cable formations: (**a**) trefoil formation; (**b**) flat formation.

In solid bonding systems (suitable for cable lengths over 500 m), the cable shields are grounded at both ends of the cables, as depicted in Figure 2, where R_g represents the grounding resistance. This bonding scheme will reduce the induced shield voltages, but there will be circulating shield currents proportional to the wire-core currents. This will cause losses in the shields, which reduce the cable current carrying capacity. At the same time, the circulating shield current generates a magnetic field that is significantly out of phase with respect to the wire-core magnetic field. In the following, only the total magnetic field will be investigated.

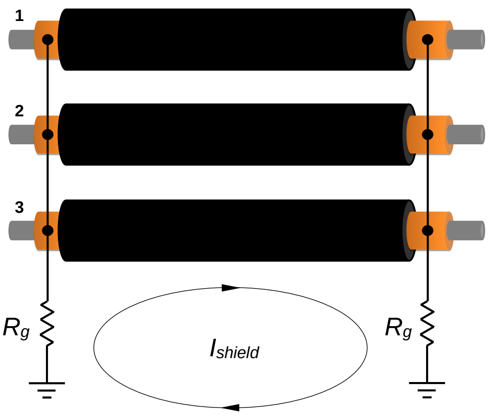

Figure 2. Solid bonding.

Since solid bonding is more common for medium-voltage applications, a 12/20 kV NA2XS(F)2Y single-core cable (Figure 3) has been selected for finite element analysis. The cable is constructed from aluminum (Al) core conductor with the cross-sectional area of 150 mm^2, semi-conductive layer over conductor, core insulation of cross-linked polyethylene (XLPE), semi-conductive layer over insulation, swelling tape, copper (Cu) wire shield with the cross-sectional area of 25 mm^2, waterproofing tape and outer sheath of high-density polyethylene (HDPE). The current carrying capacity when buried in the ground is 319 A for trefoil formation and 352 A for flat formation, respectively. Other cable characteristics are given in Table 1.

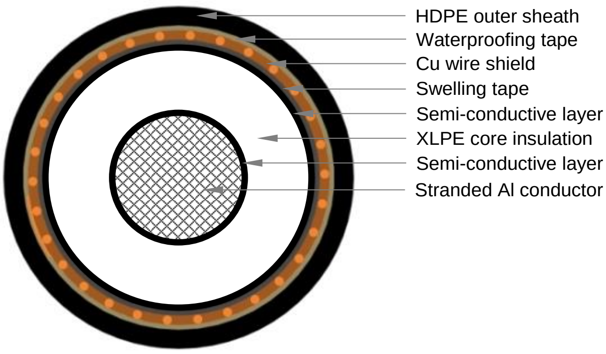

Figure 3. NA2XS(F)2Y cable.

Table 1. Cable characteristics.

Cable Characteristic	Value
Core conductor diameter	14.2 mm
Nominal cross-sectional area of core conductor	150 mm^2
Thickness of XLPE insulation	5.5 mm
Diameter over insulation	26.4 mm
Diameter over copper shield	30.5 mm
Nominal cross-sectional area of shield	25 mm^2
Diameter over HDPE sheath (over complete cable)	36 mm
Nominal phase-to-ground/phase-to-phase voltage	12/20 kV
DC resistance of conductor at 20 °C	0.206 Ω/km
Maximum operating conductor temperature	+90 °C

The physical layout of the analyzed three-phase cable system is presented in Figure 4, where two cases are considered in conformity with the national regulations regarding the design and execution of the electrical cable networks [23]:

- The three phases are buried in the ground, at a depth of 0.8 m, in trefoil formation (the spacing between the centers of any two cables is 36 mm, as dictated by the cable outer diameter), Figure 4a;
- The three phases are buried in the ground, at a depth of 0.8 m, in flat formation with clearance between cables of 70 mm (the spacing between the centers of the adjacent cables is 106 mm), Figure 4b.

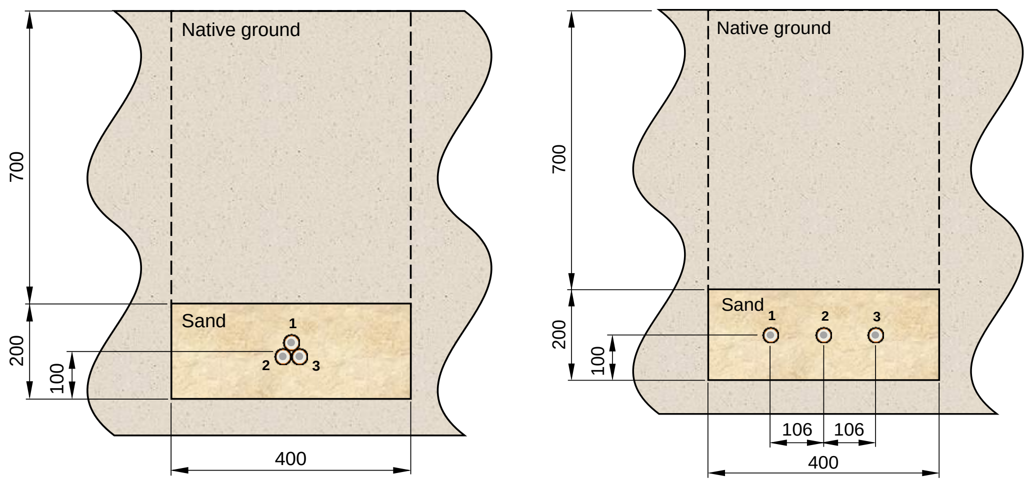

Figure 4. Physical layout of the analyzed three-phase cable system: (**a**) trefoil formation; (**b**) flat formation with spacing (all dimensions are given in mm).

In both cases, the power cables are located in a rectangular trench 0.9 m deep and 0.4 m wide, between two sand layers of 0.1 m thickness. Both ends of all cable shields are connected to ground, as indicated in Figure 2.

For model implementation and its validation, it is assumed that the three-phase cable system has exactly balanced currents, as follows: $\boldsymbol{I_1} = I \angle -120°$, $\boldsymbol{I_2} = I \angle 0°$ and $\boldsymbol{I_3} = I \angle 120°$. Computations will be performed at maximum rated current (319 A and 352 A, respectively), assuming that the actual laying depth has no significant influence on the maximum admissible load current, which is otherwise compensated by the reduction in the ambient temperature and the more favorable specific thermal resistances of the ground at bigger laying depths (according to [23], the usual laying depth range is approximately 0.7 m ÷ 1.2 m). Additionally, the surrounding ground is considered electrically homogenous and non-magnetic.

3. Finite Element Model

ANSYS Maxwell 2D is a powerful software package that uses the finite element method to solve 2D low-frequency electromagnetic problems, by specifying the appropriate geometry, material properties and excitations for a device or system of devices [24,25]. The proposed magnetic field problem is solved using the eddy current field solver, which allows computing steady state, time-varying (AC) magnetic fields at a given frequency, here 50 Hz. It also computes current densities, taking into account eddy current effects in solid conductors (including skin and proximity effects), as well as other quantities that can be derived from the magnetic field solution. An adaptive mesh refinement technique is used to achieve the best mesh required to meet the defined accuracy level.

The quantities that the eddy current field simulator resolves are the magnetic vector potential ($\boldsymbol{A}$)—related to magnetic flux density by $\boldsymbol{B} = \nabla \times \boldsymbol{A}$—and the electric scalar potential (V). A first equation used for this purpose, derived from Maxwell's equations, is:

$$\nabla \times \frac{1}{\mu}(\nabla \times \boldsymbol{A}) = (\sigma + j\omega\varepsilon)(-j\omega\boldsymbol{A} - \nabla V), \quad (1)$$

where μ is the absolute magnetic permeability, σ is the electrical conductivity, and $\omega = 2\pi f$ is the angular frequency at which all quantities are oscillating and ε is the absolute electric permittivity.

As we can see, the right side of (1) consists of a complex conductivity, $\sigma + j\omega\varepsilon$, multiplied by the complex value of the electric field strength, i.e., $\boldsymbol{E} = -j\omega\boldsymbol{A} - \nabla V$. Therefore, the result is the complex current density, $\boldsymbol{J}$, which is the sum of three components:

- $\boldsymbol{J_s} = -\sigma\nabla V$, the source current density due to the differences in electric potential;
- $\boldsymbol{J_e} = -j\omega\sigma\boldsymbol{A}$, the induced eddy current density due to time-varying magnetic fields;
- $\boldsymbol{J_d} = j\omega\varepsilon(-j\omega\boldsymbol{A} - \nabla V)$, the displacement current density due to time-varying electric fields.

Since the total current (I_T) flowing in any conductor that is connected to an external source is specified when setting up the problem, a second equation used by the eddy current module to solve for $\boldsymbol{A}$ and V is:

$$I_T = \int_S \boldsymbol{J} dS = \int_S (\sigma + j\omega\varepsilon)(-j\omega\boldsymbol{A} - \nabla V), \quad (2)$$

which basically states that the total current in a conductor equals the integral of $\boldsymbol{J}$ over the cross-sectional area of the conductor, S.

Because $\boldsymbol{B}$ is assumed to lie in the xy plane, $\boldsymbol{A}$ has only a component in the z direction. Therefore, the eddy current module will solve only for $\boldsymbol{A_z}(x,y)$. Additionally, $\boldsymbol{E}$ has a z component only, which means that V is constant over the entire cross section of a conductor. Therefore, it is not necessary to solve for V at every node.

3.1. Global FEM Model, Boundary Conditions and Solver Setup

The global FEM model of the three-phase cable system is depicted in Figure 5a, where the computational domain is a square of side a = 20 m, sufficiently large to determine the behavior of the magnetic field well outside from the cable central axis. A discretized section around the power cables is given in Figure 5b. The power cables are buried—according to the geometrical dimensions in Figure 4a (for trefoil formation) and Figure 4b (for flat formation)—in a ground with the electrical conductivity σ = 0.01 S/m, the relative magnetic permeability μ_r = 1 and the relative electric permittivity ε_r = 10. The half top layer in Figure 5a models the air. The model depth (cable length) is 1 m.

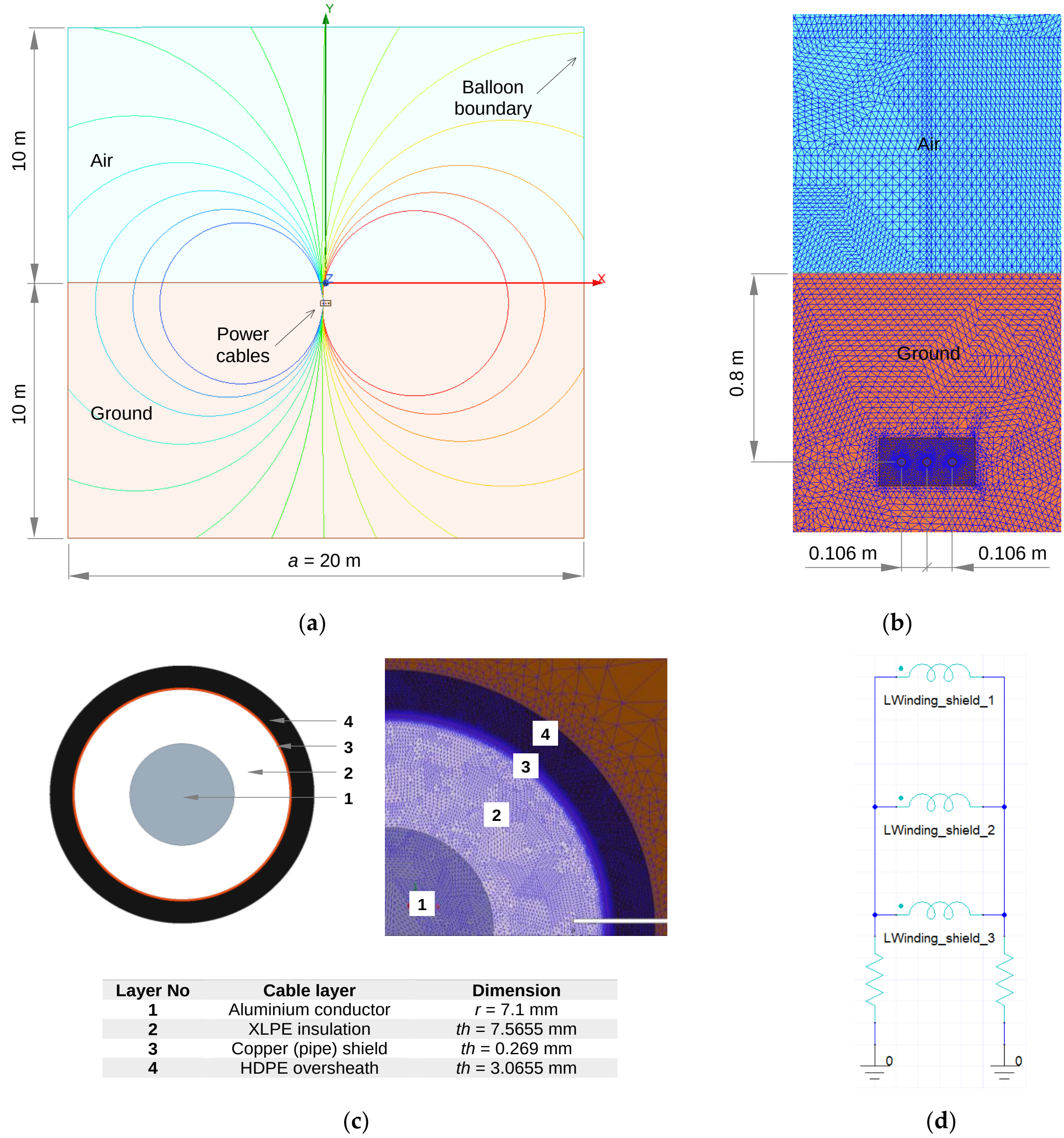

Layer No	Cable layer	Dimension
1	Aluminium conductor	*r* = 7.1 mm
2	XLPE insulation	*th* = 7.5655 mm
3	Copper (pipe) shield	*th* = 0.269 mm
4	HDPE oversheath	*th* = 3.0655 mm

Figure 5. The 2D FEM model for computing magnetic fields from a three-phase underground cable system with solid bonding: (**a**) global geometric model; (**b**) discretized section around the power cables; (**c**) simplified cable model; (**d**) coupled circuit for shield bonding.

All power cables are modeled as presented in Figure 5c, using a simplified four-layer cable model consisting of Al core conductor (σ_{20} = 35.38 $\times$ 10^6 S/m, μ_r = 1 and ε_r = 1), XLPE insulation (σ = 1 $\times$ 10^{-15} S/m, μ_r = 1 and ε_r = 2.5), Cu shield (σ_{20} = 58 $\times$ 10^6 S/m, μ_r = 1 and ε_r = 1) and HDPE oversheath (σ = 1 $\times$ 10^{-14} S/m, μ_r = 1 and ε_r = 2.3). The equivalent thickness (*th*) of the Cu shield layer is chosen so that it closely matches the nominal 25 mm^2 cross-sectional area of the real wire shield, while its mean radius is exactly the same, 14.8 mm. For cables with metallic sheets, the sheet layer in the cable model will simply reflect the cross section of the real sheet. In simulation, the aforementioned conductivities (at T_0 = 20 °C) of the metallic layers will be adjusted to maximum operating temperatures (90 °C for Al core conductors; approximately 80 °C for Cu shields), by taking into account the following temperature coefficients (of resistivity, $\rho = 1/\sigma$) per K at 20 °C [26]: 4.03 × 10^{-3} for Al and, respectively, 3.93 × 10^{-3} for Cu.

Since the analyzed cable structure is assumed to be completely isolated from other magnetic fields or sources of current, Balloon boundary conditions are assigned to all four edges of the defined computational domain. In this case, the magnetic vector potential, $\boldsymbol{A}_z$, goes to zero at infinity; the magnetic flux lines are neither tangential nor normal to the Balloon boundary. At the interfaces between objects, natural boundary conditions are automatically assigned by the eddy current module.

The values of the wire-core currents (amplitude and phase) are assigned using the software functionality "Current Excitation", while the shield bonding is encoded in the model by the coupled circuit in Figure 5d, where external windings are used for controlling the induced shield currents. This electrical circuit was defined with Maxwell Circuit Editor. As mentioned above, only perfectly balanced currents are considered for model implementation and further validation, but unbalanced loading conditions can also be managed. By simulation, the effect of grounding resistance was proved to be insignificant.

A fine mesh was defined for analysis, totalizing a number of triangle elements in the order of 1,300,000. The mesh refinement was achieved by restricting the maximum length of the elements in all model blocks, ensuring that high-resolution magnetic field profiles are generated over a large distance of interest with respect to the cable central axis (a number of preliminary tests with mesh size were performed). The maximum element length in the (very thin) shield blocks is 0.05 mm, which represents the minimum defined over the entire domain. In the air and surrounding ground, the maximum element length is 60 mm, which represents the maximum defined over the entire domain.

The adaptive setup was configured with a maximum number of passes of 10 and a percent error of 0.1. The convergence was set as 30% refinement per pass, minimum number of passes of 2 and minimum number of converged passes of 1. The adaptive frequency is 50 Hz.

3.2. Calculation of RMS Magnetic Flux Density

According to the usual evaluation procedures applied in magnetic field exposure studies, we are mainly interested in computing lateral profiles of the RMS magnetic flux density at various heights above the ground, particularly at the standard height of 1 m. Such profiles of B_{RMS} are calculated in a separate Microsoft Excel worksheet, where a sufficiently large number of instantaneous magnetic flux density profiles (generated over a 20-ms period) are imported and then "summed" together with the formula [18,27]:

$$B_{RMS}(i) = \sqrt{\frac{1}{N}\sum\nolimits_{n=1}^{N} B_n^2(i)}, \tag{3}$$

where $B_1(i), \ldots, B_N(i)$ are the instantaneous values of the magnetic flux density corresponding to the point i of the profile and N stands for the total number of values (profiles). Here, we use N = 73.

On this basis, for I = 319 A, Figure 6a shows lateral profiles of the instantaneous magnetic flux density up to 10 m from the central axis of the three-phase power cable in trefoil formation, at the height of 1 m above the ground, as well as the correspondent B_{RMS} profile (blue thick line). A 2D distribution of the instantaneous magnetic flux density around the three-phase cable in trefoil formation (at the time t = 16.94 ms, at which the peak magnetic flux density in Figure 6a is obtained) is presented in Figure 6b. Similarly, by adopting I = 352 A, Figure 7a shows simulation results for the three-phase power cable in flat formation. A 2D distribution of the instantaneous magnetic flux density around the three-phase cable in flat formation (at the time t = 15.56 ms, at which the peak magnetic flux density in Figure 7a is obtained) is depicted in Figure 7b. More details on the magnetic fields and induced shield currents from both configurations are discussed in Section 5.

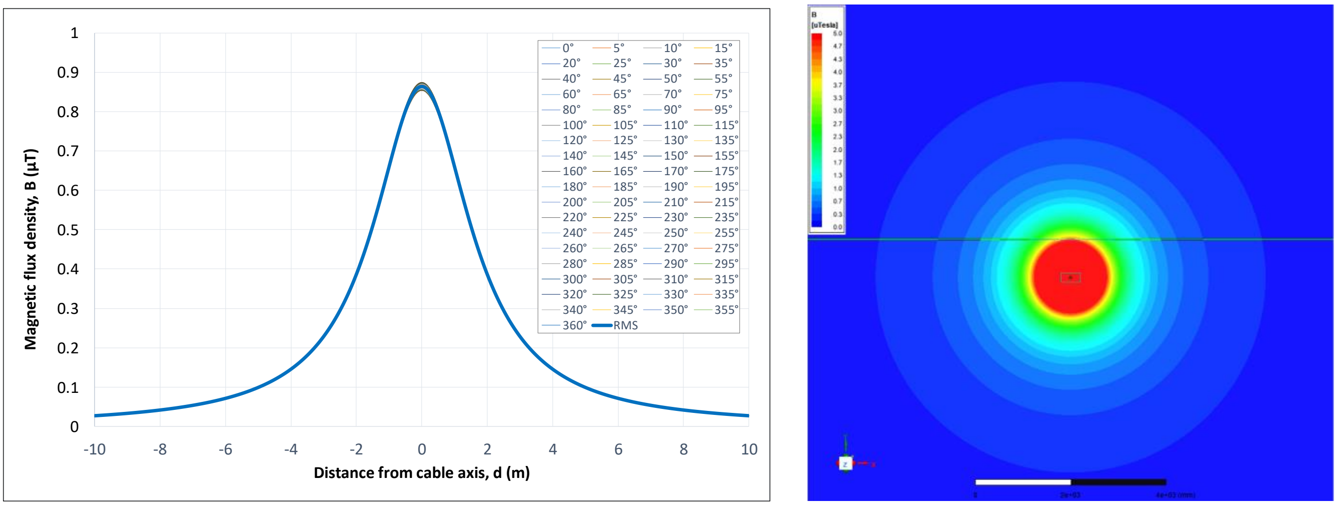

(**a**) (**b**)

Figure 6. Example of simulation results for the three-phase power cable in trefoil formation: (**a**) instantaneous magnetic flux density profiles and calculated RMS magnetic flux density profile at the height h = 1 m above the ground; (**b**) a momentary magnetic field distribution in the cross section of the power cable (t = 16.94 ms).

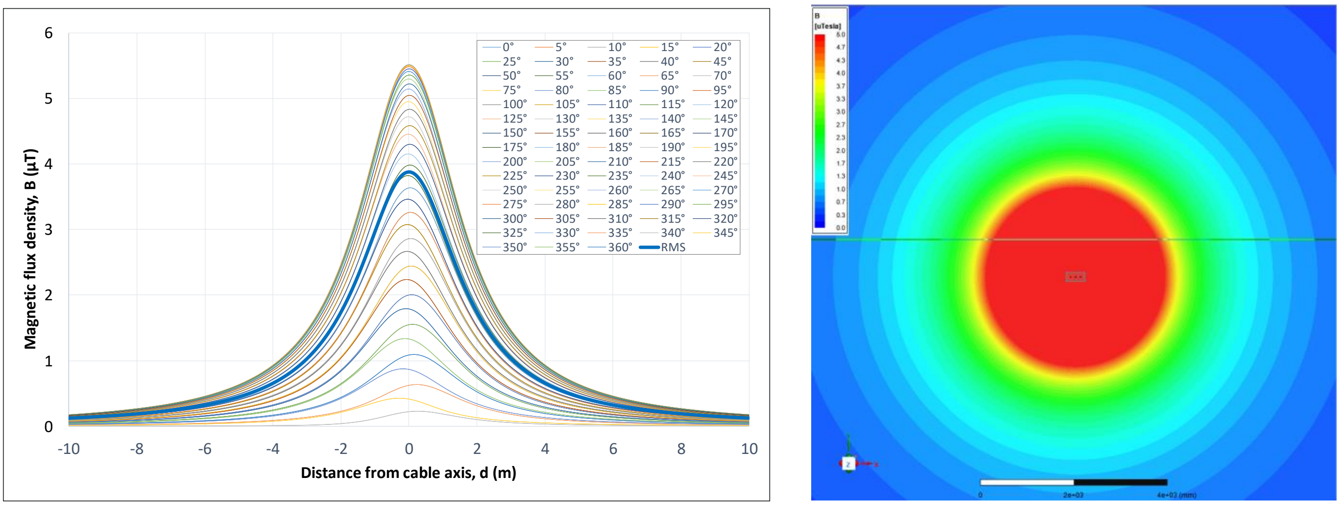

(**a**) (**b**)

Figure 7. Example of simulation results for the three-phase power cable in flat formation: (**a**) instantaneous magnetic flux density profiles and calculated RMS magnetic flux density profile at the height h = 1 m above the ground; (**b**) a momentary magnetic field distribution in the cross section of the power cable (t = 15.56 ms).

4. Analytical Approach for FEM Model Validation

To verify the numerical results obtained with the proposed FEM model, an interactive software tool based on the Biot–Savart law and the superposition principle has been developed. Assuming that the power cables are straight and infinitely long, the total magnetic flux density at any measuring point (x, y) in the vicinity of a three-phase power cable with solid bonding can be calculated as (Figure 8):

$$B_x = \sum_{i=1}^{3} \frac{-\mu_0}{2\pi}(I_i + I_{sh\_i})\left[\frac{y - y_i}{r_i^2}\right]; \tag{4}$$

$$B_y = \sum_{i=1}^{3} \frac{\mu_0}{2\pi}(I_i + I_{sh\_i})\left[\frac{x - x_i}{r_i^2}\right]; \tag{5}$$

$$B = \sqrt{|B_x|^2 + |B_y|^2}, \tag{6}$$

where I_i is the phase current carried by the conductor located at (x_i, y_i), I_{sh_i} is the circulating current in the shield located at (x_i, y_i), $r_i = \sqrt{(x - x_i)^2 + (y - y_i)^2}$ represents the distance between the conductor/shield and the measurement point (x, y) and $\mu_0 = 4\pi \times 10^{-7}$ H/m is the magnetic permeability of the free space.

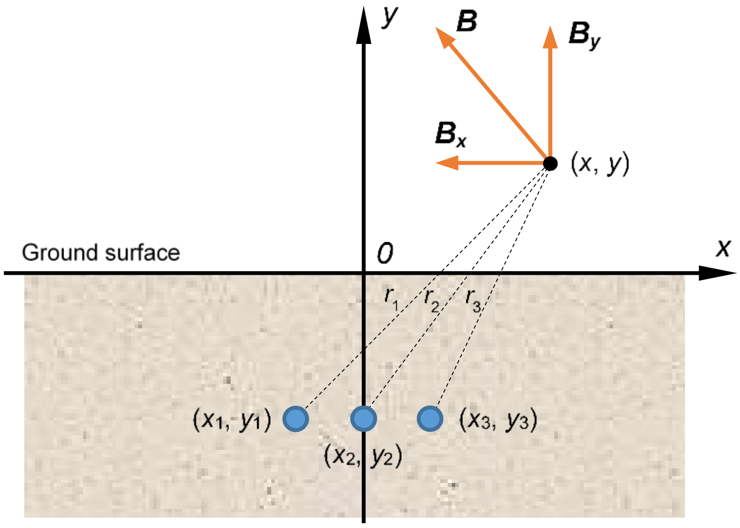

Figure 8. The 2D analytical calculation of the magnetic flux density generated by a three-phase power cable with solid bonding.

If considering the same phase sequence ($I_1 = I\angle{-120°}$, $I_2 = I\angle 0°$ and $I_3 = I\angle 120°$), it can be shown that the currents induced in the shields of the three-phase power cable in trefoil formation (Figure 1a) have the general form [21,26]:

$$I_{sh\_i} = -I_i \frac{jX}{R_{sh} + jX}, \tag{7}$$

where $X = 2 \times \omega \times 10^{-7} \ln(s/r_{sh})$ represents the shield reactance per unit length of cable, in Ω /m, and R_{sh} is the shield DC resistance per unit length of cable, in Ω/m. In the expression of X, s is the spacing between the centers of the (adjacent) conductors, in m, and r_{sh} is the mean of the outer and inner radii of the shield, in m.

Similarly, for balanced phase currents, the currents induced in the shields of the three-phase power cable in flat formation (Figure 1b) have the following expressions [21,26]:

$$I_{sh\_1} = \frac{I_2}{2}\left[\frac{Q^2}{R_{sh}^2 + Q^2} - \frac{\sqrt{3}R_{sh}P}{R_{sh}^2 + P^2} + j\left(\frac{R_{sh}Q}{R_{sh}^2 + Q^2} + \frac{\sqrt{3}P^2}{R_{sh}^2 + P^2}\right)\right]; \tag{8}$$

$$I_{sh\_2} = -I_2\left(\frac{Q^2}{R_{sh}^2 + Q^2} + j\frac{R_{sh}Q}{R_{sh}^2 + Q^2}\right); \tag{9}$$

$$I_{sh\_3} = \frac{I_2}{2}\left[\frac{Q^2}{R_{sh}^2 + Q^2} + \frac{\sqrt{3}R_{sh}P}{R_{sh}^2 + P^2} + j\left(\frac{R_{sh}Q}{R_{sh}^2 + Q^2} - \frac{\sqrt{3}P^2}{R_{sh}^2 + P^2}\right)\right], \tag{10}$$

where $Q = X - X_m/3$, $P = X + X_m$, $X = 2 \times \omega \times 10^{-7} \ln(s/r_{sh})$ represents the shield reactance per unit length of cable for two adjacent single-core cables, in Ω/m, and $X_m = 2 \times \omega \times 10^{-7} \ln 2$ is the mutual reactance per unit length of cable between the shield of an outer cable and the conductors of the other two, in Ω/m.

Finally, the shield resistance R_{sh} (at the shield temperature T_{sh}) is calculated with the formula:

$$R_{sh} = \frac{\rho_{sh20}}{A_{sh}}[1 + \alpha_{sh20}(T_{sh} - 20)], \quad (11)$$

where ρ_{sh20} is the electrical resistivity of the shield material at 20 °C, A_{sh} is the shield cross-sectional area and α_{sh20} is the temperature coefficient of resistance at 20 °C. In our case, at T_{sh} = 80 °C, R_{sh} = 0.852 mΩ/m.

All these equations, together with a field mapping algorithm, have been implemented into a LabVIEW program that is able to generate lateral profiles of the total RMS magnetic flux density, B, as well as of its transversal components, B_x and B_y, at any user-defined height above the ground. The program also displays the induced shield currents (RMS value and phase). Magnetic flux density profiles generated with this simulation tool for trefoil formation (I = 319 A) and flat formation (I = 352 A) are presented in Figure 9a,b, respectively. Detailed comparisons to numerical results are presented in Section 5.

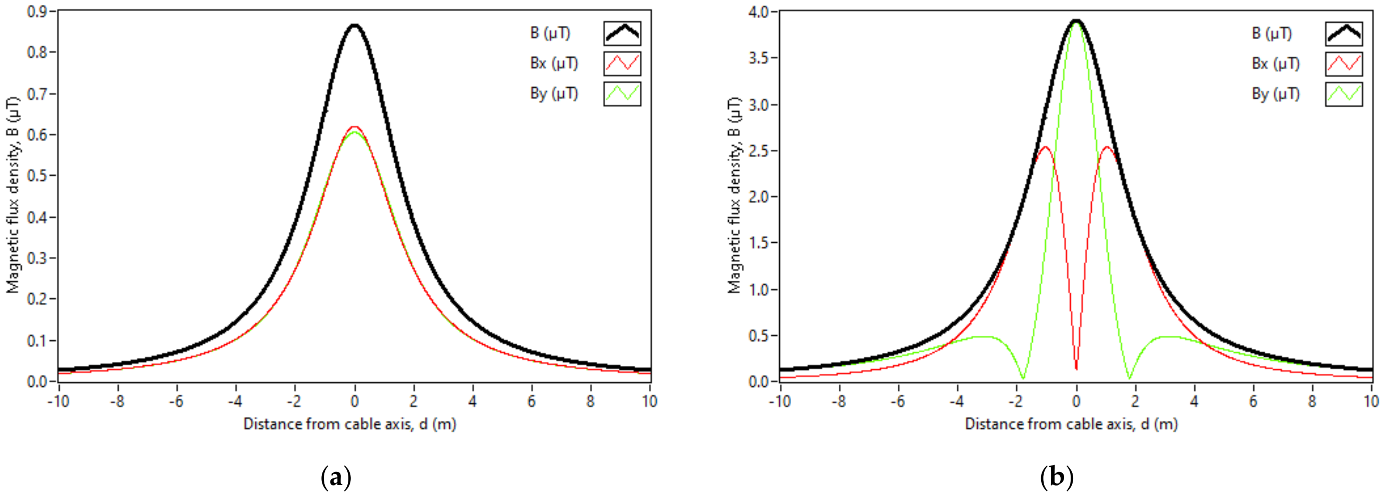

Figure 9. Example of results obtained by analytical computation (the total RMS magnetic flux density and its transversal components at the height of 1 m above the ground): (**a**) for the three-phase power cable in trefoil formation; (**b**) for the three-phase power cable in flat formation.

5. Results and Discussions

5.1. Magnetic Fields from the Considered Trefoil and Flat Formations

Comparisons between FEM simulation results and analytical computation results (lateral profiles of the total RMS magnetic flux density at the height of 1 m above the ground) for the considered trefoil and flat formations are given in Figure 10a,b, respectively. Induced shield currents calculated by both methods are given in Tables 2 and 3, respectively. As it can be seen, the results obtained by the two methods correlate very well. The smallest difference in the RMS magnetic flux density at the cable central axis is obtained for trefoil formation (Figure 10a), namely 2.36 nT. For the three-phase underground power cable in flat formation (Figure 10b), the difference in RMS magnetic flux density at the centerline is 26.49 nT. In both cases, lower values of magnetic flux density have been obtained by numerical simulation. Clearly, these differences are too small for any practical purposes related to magnetic field exposure assessment, but we may assume a slightly different evaluation of the electromagnetic interaction between models (eddy currents in shields are neglected in the analytical model).

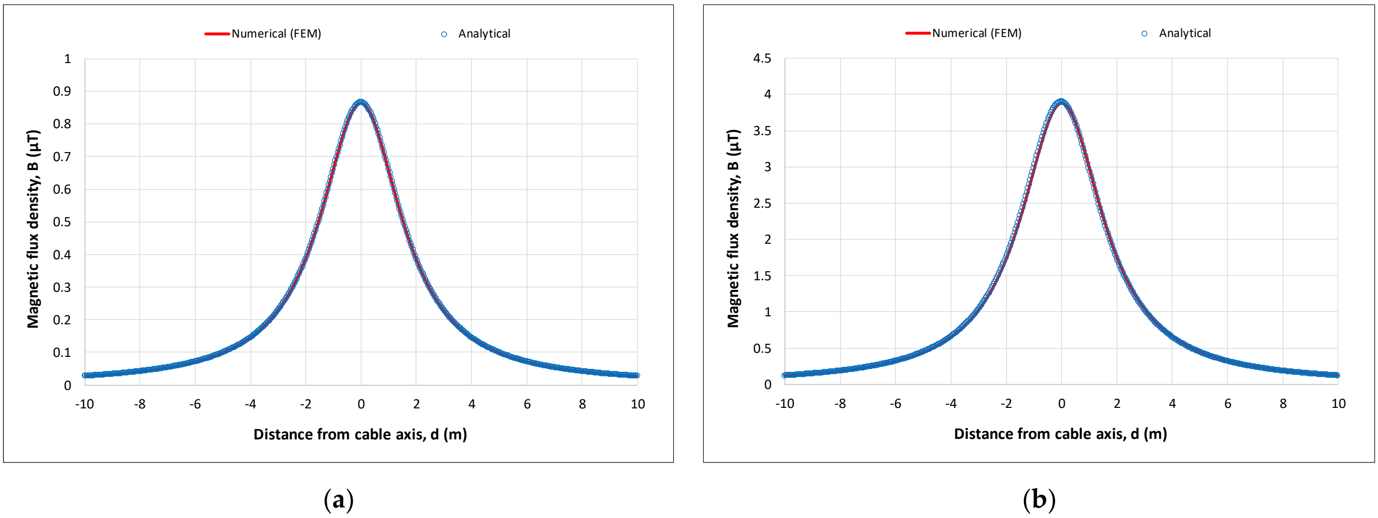

Figure 10. Comparison between numerical and analytical results (RMS magnetic flux density profiles at the height of 1 m above the ground): (**a**) for the three-phase power cable in trefoil formation; (**b**) for the three-phase power cable in flat formation.

Table 2. Induced shield currents obtained by numerical simulation and analytical computation (trefoil formation).

Current No.	Conductor Current		Shield Current (FEM)		Shield Current (Analytical)	
	RMS Value (A)	Phase (°)	RMS Value (A)	Phase (°)	RMS Value (A)	Phase (°)
1	319	–120	20.816	145.371	20.872	146.248
2	319	0	20.814	–94.625	20.872	–93.752
3	319	120	20.814	25.368	20.872	26.248

Table 3. Induced shield currents obtained by numerical simulation and analytical computation (flat formation).

Current No.	Conductor Current		Shield Current (FEM)		Shield Current (Analytical)	
	RMS Value (A)	Phase (°)	RMS Value (A)	Phase (°)	RMS Value (A)	Phase (°)
1	352	–120	64.129	148.533	64.229	148.547
2	352	0	44.704	–97.308	44.757	–97.305
3	352	120	61.347	10.178	61.454	10.196

Decreasing the number of mesh elements to about 620,000 still produces very accurate results in the RMS magnetic flux density (differences below 0.04% at the height of 1 m above the ground, regardless the measurement point), while the computation time reduces from about 25 min to 10 min (Intel® Core™ i7-12700H Processor, 14 CPU, 16 GB RAM, GeForce RTX 3050 GPU). Doubling and even tripling the number of mesh elements has no significant effect on the calculated RMS magnetic flux density profile at the height of 1 m above the ground.

With the setting of Balloon boundary conditions, the distance from the source of magnetic fields (cables) to the outer boundary is not a critical issue, since different dimensions of boundary has almost no effect on the simulation results (for instance, the simulation results obtained by doubling the side *a* of the computational domain are virtually identical). If the side *a* of the computational domain reduces to half, the differences in the RMS magnetic flux density at the height of 1 m above the ground, regardless the measurement point, do not exceed 0.06%.

Lateral profiles of the total RMS magnetic flux density at several heights above the ground, obtained by numerical simulation only, are presented in Figure 11a,b, respectively.

At maximum rated current (319 A), the magnetic field at the central axis of the three-phase power cable in trefoil formation is very low compared to the ICNIRP 1998 limit for general public (100 µT at 50 Hz) [28], ranging from 4.377 µT at the ground level (0-m height) to 0.357 µT at the height of 2 m. At the standard height of 1 m, the RMS magnetic flux density at the centerline is 0.864 µT (115.74-fold below the ICNIRP reference level), while at the distance of 10 m from the cable axis it falls to only 0.027% of the ICNIRP limit. Much higher exposure levels can be observed for the three-phase power cable in flat formation (maximum rated current of 352 A), in which case the RMS magnetic flux density above the cable axis varies from 19.409 µT at 0-m height to 1.604 µT at the height of 2 m. Once again, at the standard height of 1 m, the RMS magnetic flux density at the centerline is 3.876 µT (25.8-fold below the ICNIRP reference level), falling to 0.122% of the ICNIRP limit at the distance of 10 m from the cable axis. These values should be seen as maximum exposure levels from such common configurations of 12/20 kV three-phase underground power cables.

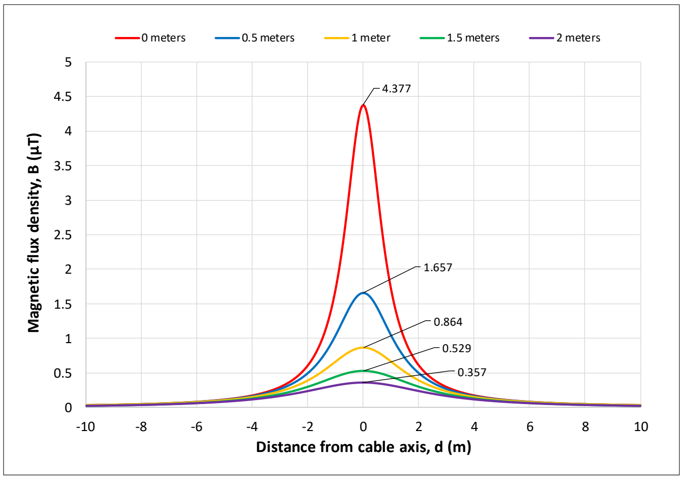

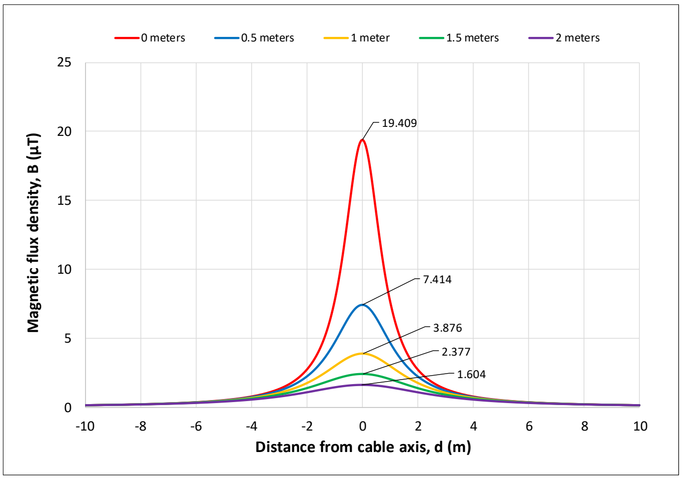

(**a**) (**b**)

Figure 11. Magnetic flux density profiles at several heights above the ground, obtained by numerical simulation: (**a**) for trefoil formation; (**b**) for flat formation.

To illustrate the effect of shields on the magnetic field reduction, Figure 12a,b compare vertical profiles of the total RMS magnetic flux density at the central axis of the two analyzed cable structures, obtained by numerical simulation, with solidly bonded and non-bonded shields. As shown in Figure 12a, for trefoil formation, the underground cable with solidly bonded shields produces a magnetic field that is only 0.41% lower than the magnetic field created by the non-bonded cable. For flat cable formation (Figure 12b), the magnetic field reduction effect is more evident, namely 1.83%. If we theoretically assume that both the core conductors and shields operate at a temperature of 20 °C (hence they exhibit lower resistivity, see Section 3), these figures increase to 0.62% and 2.76%, respectively.

As it can be observed from the results presented above, the magnetic field reduction rate for the analyzed cable configurations is quite low. However, for other cable systems, depending on their geometry and the cable characteristics, it may significantly increase. For instance, if we replace the 12/20 kV NA2XS(F)2Y single-core cable used in the FEM model with a similar one, but having a copper wire shield with the cross-sectional area of 50 mm^2, the RMS magnetic flux density at the central axis of the two three-phase power cables will have the vertical profiles given in Figures 13a and 13b, respectively. Now, for trefoil formation, the underground cable with solidly bonded shields generates a magnetic field that is 1.45% lower than the magnetic field created by the non-bonded cable (Figure 13a), while the magnetic field reduction rate for flat formation increases to 6.76% (Figure 13b).

At a temperature of 20 °C for both the core conductors and shields, the magnetic field reduction rates increase to 2.24% and 9.82%, respectively.

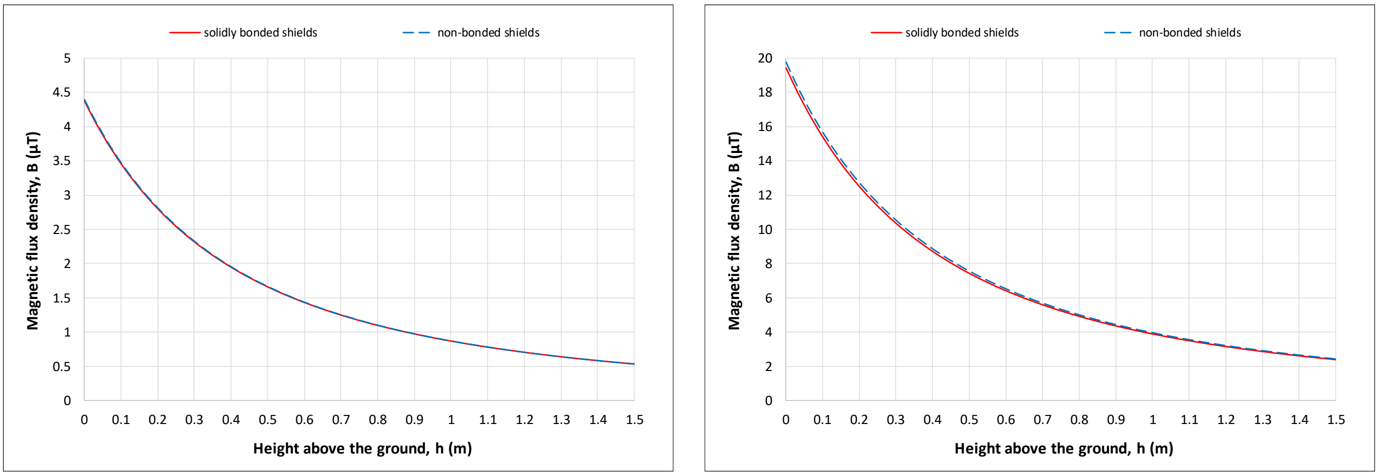

(**a**) (**b**)

Figure 12. Magnetic flux density at the central axis of the three-phase power cable with solidly bonded shields and non-bonded shields, obtained by numerical simulation: (**a**) for trefoil formation; (**b**) for flat formation.

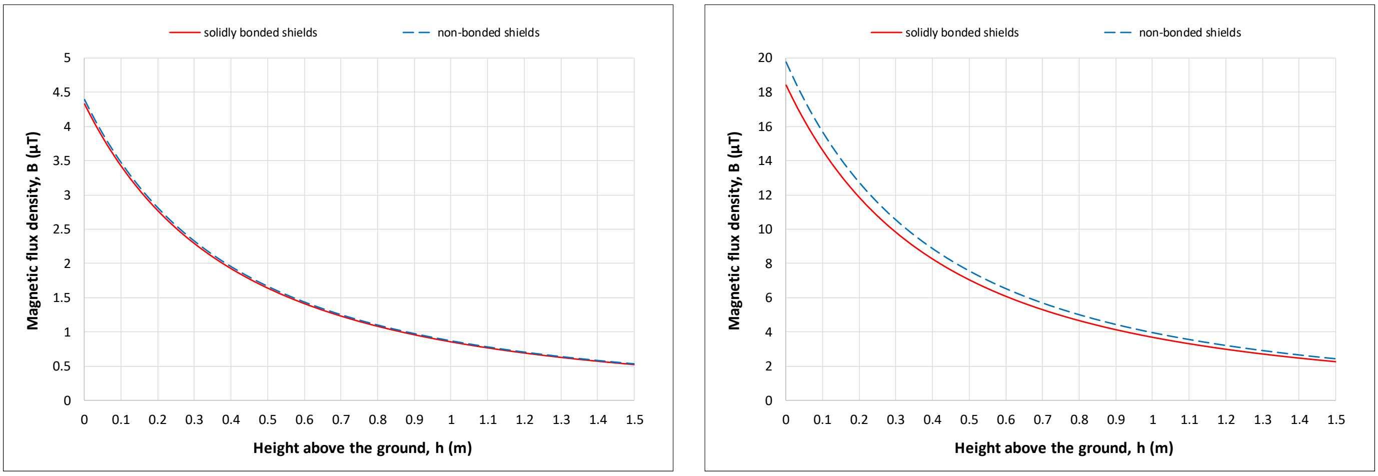

(**a**) (**b**)

Figure 13. Magnetic flux density at the central axis of the three-phase underground power cable with solidly bonded shields and non-bonded shields (50 mm^2 copper wire shield), obtained by numerical simulation: (**a**) for trefoil formation; (**b**) for flat formation.

Compared to FEM, the software based on standard formulas provides much faster results, but it can only be applied to simple trefoil and flat formations of underground power cables (under balanced loading conditions). On the other hand, FEM is much more flexible, allowing to take into consideration different cable aspects (armoring, current unbalance, etc.), and it can easily be extended to various types of cable arrangements. Such an example will be presented in the following.

5.2. Magnetic Field from Two Adjacent Three-Phase Power Cables in Flat Formation

After FEM model validation, it was used to investigate the magnetic flux density distribution and magnetic field reduction rate for an arrangement of two adjacent three-phase power cables (with solid bonding) laid horizontally in the ground, also at the burial depth of 0.8 m (Figure 14). Each individual cable is modeled as presented in Figure 5c. According to [23], the clearance between cables is 70 mm, hence the spacing between the centers of the adjacent cables is 0.106 m. It is assumed that both circuits carry (maximum) balanced currents of 307 A_{RMS} (a correction factor has been applied for cable agglomeration) and the temperatures of all core conductors and shields are 90 °C and 80 °C, respectively. For analysis, the phases of the left-side circuit are indicated by the letters A, B and C, while the phases of the right-side circuit are indicated by the letters A′, B′ and C′.

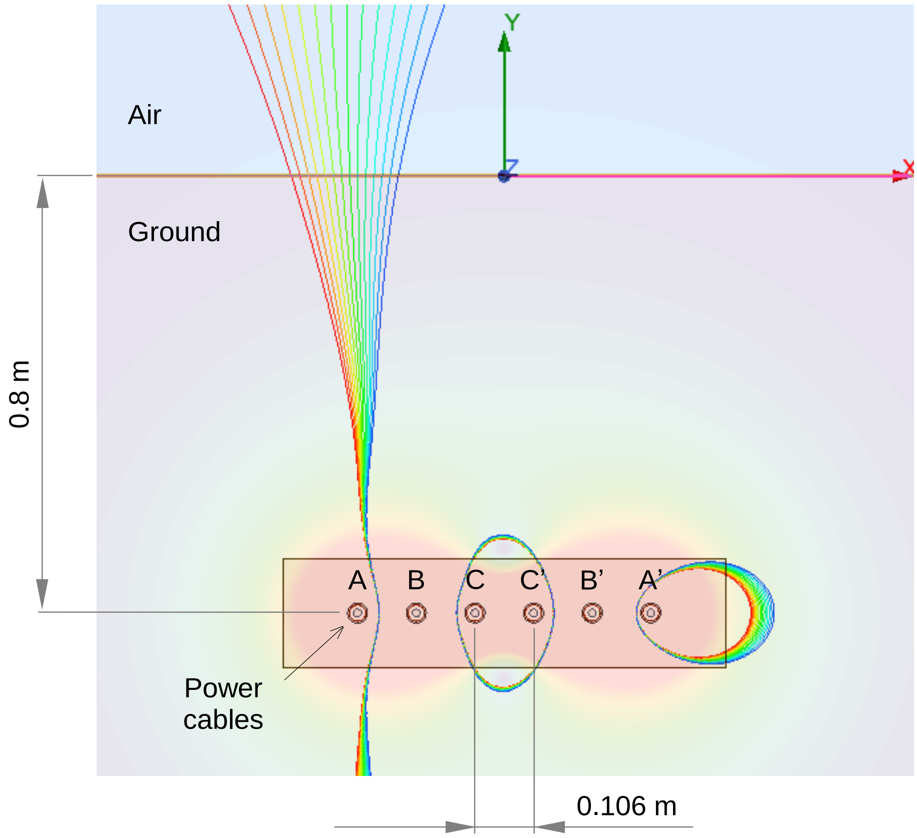

Figure 14. The 2D FEM model for computing magnetic fields from an arrangement of two adjacent three-phase power cables (with solid bonding) in flat formation.

Generally, the magnetic fields generated by two or more adjacent three-phase underground power cables will interact in a complex way, depending on their relative phase sequences and positions. Figure 15 shows the variations of RMS magnetic flux density at the height of 1 m above the ground with the change in phase sequence of the two adjacent three-phase power cables. The maximum RMS magnetic flux density, 6.633 µT, is obtained when the phases of the two circuits are in the same order, respectively ABC-A′B′C′. On the contrary, the minimum RMS magnetic flux density, 1.213 µT, is obtained when the phases of the two circuits are in reversed order, respectively ABC-C′B′A′. This confirms what some industry guidelines recommend for two parallel three-phase circuits. A 2D distribution of the instantaneous magnetic flux density around the analyzed cable arrangement is given in Figure 16.

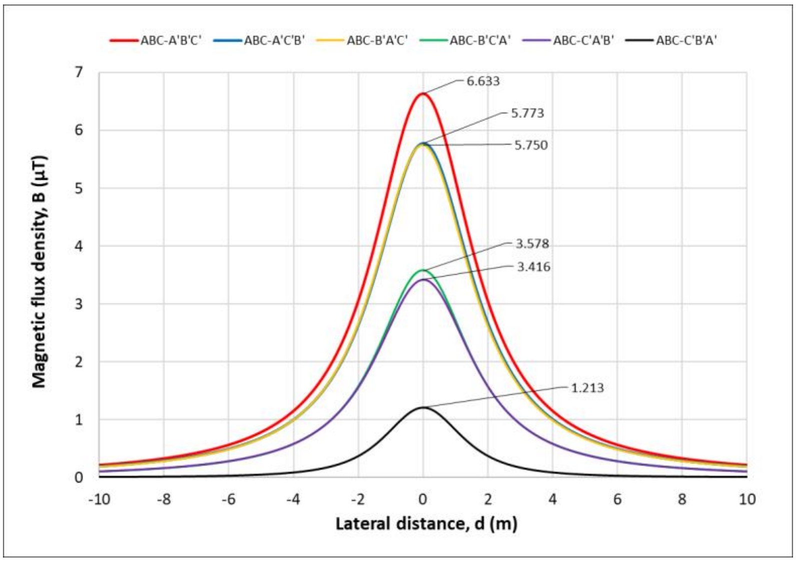

Figure 15. RMS magnetic flux density profiles at the height of 1 m above the ground as a function of phase sequence.

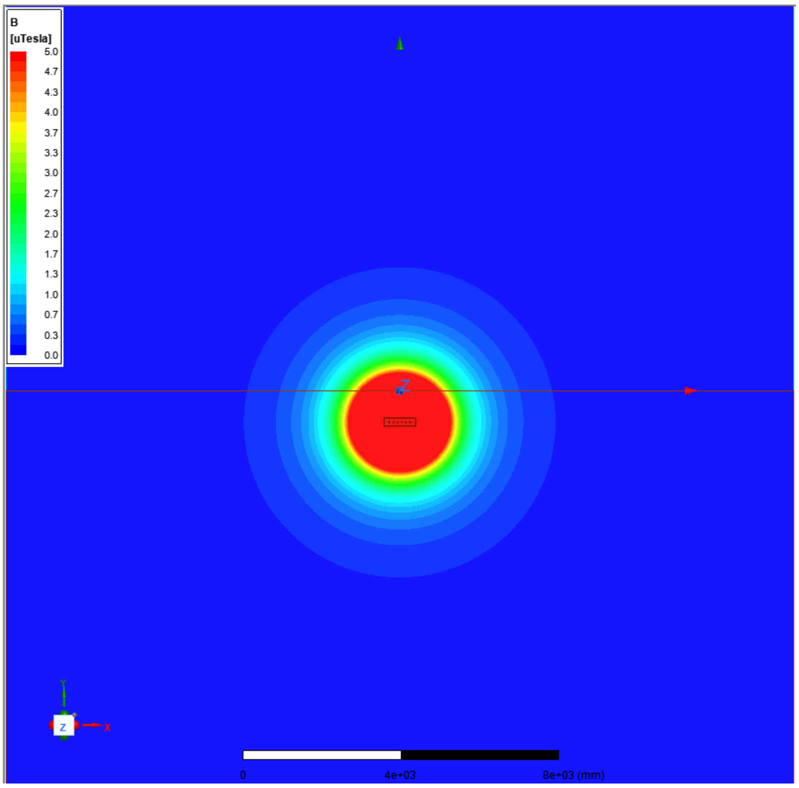

Figure 16. The 2D distribution of the (maximum) instantaneous magnetic flux density around the considered power cable arrangement.

The effect of cable shields on magnetic field reduction (at the height of 1 m above the ground) is illustrated in Table 4. The highest reduction rate, 2.16%, is obtained for the phase sequence ABC-B′A′C′, while the minimum reduction rate, 0.20%, is obtained for the phase sequence ABC-C′B′A′. However, in this case, as already presented in Figure 15, the cancelation effect in the total magnetic field created by the two circuits is maximum. At the ground level, the magnetic field reduction rate for the phase sequences ABC-B′A′C′ and ABC-C′B′A′ increases (slightly) to 2.24% and 0.33%, respectively.

Table 4. Magnetic field reduction rate due to the shields for the arrangement of two horizontally laid three-phase power cables with solid bonding.

Sequence No.	Phase Sequence		Magnetic Field Reduction Rate at 1 m above the Ground
	Left Circuit	Right Circuit	
1	ABC	A′B′C′	1.45%
2	ABC	A′C′B′	1.77%
3	ABC	B′A′C′	2.16%
4	ABC	B′C′A′	1.62%
5	ABC	C′A′B′	1.52%
6	ABC	C′B′A′	0.20%

Based on a similar analysis, numerical computations performed for an arrangement of two adjacent three-phase power cables in trefoil formation, separated by a horizontal clearance of 250 mm at the burial depth of 0.8 m [23], revealed maximum RMS magnetic flux densities (at the height of 1 m above the ground) ranging from 1.502 μT, for the phase sequence ABC-A′B′C′, to 0.517 μT, for the phase sequence ABC-B′C′A′ (optimum phasing). The highest magnetic field reduction rate, 0.50%, is obtained for the phase sequence ABC-B′A′C′, while the minimum magnetic field reduction rate, 0.40%, is obtained for the phase sequences ABC-A′B′C′ and ABC-C′A′B′. The calculated current rating of the two circuits was 284 A_{RMS}.

As we can see, the magnetic field produced by the two arrangements (for optimum phasing) is lower than the magnetic field associated with the simple cable formations discussed in the previous section. For both arrangements, the highest magnetic field reduction rate (due to induced shield currents) is not obtained for the optimum phasing.

6. Conclusions

The main achievements of this study are the development and validation of a simple and yet effective FEM model, based on ANSYS Maxwell (2D), for computing and analyzing low-frequency magnetic fields generated by three-phase underground cable systems with solid bonding. Comparisons to analytical computations based on the Biot–Savart law and the superposition principle, for both trefoil and flat formations of cables, revealed a very good agreement between results (for instance, at the standard height of 1 m above the ground, the differences in the RMS magnetic flux density at the central axis of the analyzed cable formations are only 2.36 nT and 26.49 nT, respectively).

The effect of cable shields on the magnetic field reduction has also been investigated. At maximum rated current (under balanced loading conditions), the magnetic field reduction rate due to induced shield currents is clearly better for flat cable formation, but the remaining magnetic field is significantly higher than for trefoil cable configuration. A similar situation has also been observed for an arrangement of two adjacent three-phase power cables, first laid in flat formation and then laid in trefoil formation. However, in both cases investigated here, the highest magnetic field reduction rate (due to induced shield currents) is not obtained for the optimum (low magnetic field) phasing of the two circuits.

The proposed FEM model can be adapted to calculate magnetic field distributions for any cable layout, as well as for various types of cable groups, taking into account influencing factors such as cable spacing, burial depth, phase sequence, magnetic permeability of soil. Generally, it may be used as an accurate tool for determining the worst-case magnetic field exposure levels produced by three-phase underground power cables close to the ground surface and for optimizing cable layout and location to mitigate magnetic field problems.

Author Contributions: Conceptualization, E.L., S.V. and A.S.; methodology, E.L. and S.V.; software, E.L. and S.V.; validation, E.L., S.V. and A.S.; formal analysis, E.L., S.V. and A.S.; investigation, E.L., S.V. and A.S.; resources, E.L., S.V. and A.S.; data curation, E.L., S.V. and A.S.; writing—original draft preparation, E.L., S.V. and A.S.; writing—review and editing, E.L. and A.S., visualization, E.L. and S.V.; supervision, E.L. and A.S. All authors have read and agreed to the published version of the manuscript.

Funding: This research received no external funding. The APC was funded by "Gheorghe Asachi" Technical University of Iasi.

Institutional Review Board Statement: Not applicable.

Informed Consent Statement: Not applicable.

Data Availability Statement: Not applicable.

Conflicts of Interest: The authors declare no conflict of interest.

References

1. Kljajic, D.; Djuric, N.; Bjelica, J.; Milutinov, M.; Kasas-Lazetic, K.; Antic, D. Utilization of the boundary exposure assessment for the broadband low-frequency EMF monitoring. *Meas. J.* **2017**, *100*, 110–114. [CrossRef]
2. Underground Power Cables. Available online: https://www.emfs.info/sources/underground/ (accessed on 20 April 2023).
3. Ippolito, M.G.; Puccio, A.; Ala, G.; Ganci, S. Attenuation of low frequency magnetic fields produced by HV underground power cables. In Proceedings of the 50th International Universities Power Engineering Conference (UPEC), Stoke on Trent, UK, 1–4 September 2015. [CrossRef]
4. Djekidel, R.; Mahi, D.; Hadjaj, C. Assessment of magnetic induction emission generated by an underground HV cable. *UPB Sci. Bull. C Electr. Eng. Comput. Sci.* **2016**, *78*, 179–194.
5. Kumru, C.F.; Arabul, A.Y. Numerical analysis and comparison of magnetic fields caused by constant and time varying currents in medium voltage underground cables. *Eur. J. Sci. Technol.* **2022**, *35*, 449–454. [CrossRef]
6. Ates, K.; Carlak, H.F.; Ozen, S. Magnetic field exposures due to underground power cables: A simulation study. In Proceedings of the 2nd World Congress on Electrical Engineering and Computer Systems and Science (EECSS'16), Budapest, Hungary, 16–17 August 2016. [CrossRef]
7. Abu Zarim, Z.A.; Anthony, T.M. Magnetic field simulation & measurement of underground cable system inside duct bank. In Proceedings of the 22nd International Conference on Electricity Distribution (CIRED 2013), Stockholm, Sweden, 10–13 June 2013.
8. Mahariq, I.; Beryozkina, S.; Mohammed, H.; Kurt, H. On the eddy current losses in metallic towers. *Int. J. Renew. Energy Dev.* **2020**, *9*, 1–6. [CrossRef]
9. Fernandez, E.; Patrick, J. Magnetic Fields from High Voltage Power Cables. Available online: http://elek.com.au/wp-content/uploads/2018/09/Magnetic-Fields-from-High-Voltage-Power-Cables.pdf (accessed on 20 April 2023).
10. Hernández Jiménez, V.J.; Castronuovo, E.D.; Sánchez Rodríguez-Morcillo, I. Optimal statistical calculation of underground cable bundles positions for time-varying currents. *Int. J. Electr. Power Energy Syst.* **2018**, *95*, 26–35. [CrossRef]
11. Djekidel, R.; Mahi, D.; Bessedik, S.A.; Hadjaj, C. Analysis of magnetic flux density generated by a three-phase underground power cable. In Proceedings of the 10th National Conference on High Voltage (CNHT), Algiers, Algeria, 24–26 May 2016. [CrossRef]
12. Farag, A.S.; Hossam-Eldin, A.A.; Karawia, H.M. Magnetic fields management for underground cables structures. In Proceedings of the 21st International Conference on Electricity Distribution (CIRED 2011), Frankfurt, Germany, 6–9 June 2011.
13. Rozov, V.; Grinchenko, V.; Tkachenko, O.; Yerisov, A. Analytical calculation of magnetic field shielding factor for cable line with two-point bonded shields. In Proceedings of the 2018 IEEE 17th International Conference on Mathematical Methods in Electromagnetic Theory (MMET), Kyiv, Ukraine, 2–5 July 2018. [CrossRef]
14. Riba Ruiz, J.R.; Alabern Morera, X. Effects of the circulating sheath currents in the magnetic field generated by an underground power line. In Proceedings of the International Conference on Renewable Energy and Power Quality (ICREPQ'06), Palma de Mallorca, Spain, 5–7 April 2006. [CrossRef]
15. Grinchenko, V.; Tkachenko, O.; Chunikhin, K. Magnetic field calculation of cable line with two-point bonded shields. In Proceedings of the 2017 IEEE International Young Scientists Forum on Applied Physics and Engineering (YSF), Lviv, Ukraine, 17–20 October 2017. [CrossRef]
16. Dubitsky, S.; Greshnyakov, G.; Korovkin, N. Refinement of underground power cable ampacity by multiphysics FEA simulation. *Int. J. Energy Res.* **2015**, *9*, 12–19.
17. Novák, B.; Koller, L.; Berta, I. Loss reduction in cable sheathing. In Proceedings of the International Conference on Renewable Energies and Power Quality (ICREPQ'10), Granada, Spain, 23–25 March 2010. [CrossRef]
18. Lunca, E.; Vornicu, S.; Salceanu, A. Numerical modelling of the magnetic fields generated by underground power cables with two-point bonded shields. In Proceedings of the 25th IMEKO TC4 International Symposium (IMEKO TC-4 2022), Brescia, Italy, 12–14 September 2022.
19. Vornicu, S.; Lunca, E.; Salceanu, A. Computation of the low frequency magnetic fields generated by a 12/20 kV underground power line. In Proceedings of the 2018 International Conference and Exposition on Electrical and Power Engineering (EPE), Iasi, Romania, 18–19 October 2018. [CrossRef]
20. Mahariq, I.; Erciyas, A. A spectral element method for the solution of magnetostatic fields. *Turk. J. Elec. Eng. Comp. Sci.* **2017**, *25*, 2922–2932. [CrossRef]
21. Gouda, O.E. *Environmental Impacts on Underground Power Distribution*, 1st ed.; IGI Global: Hershey, PA, USA, 2016.
22. Ocłoń, P.; Cisek, P.; Pilarczyk, M.; Taler, D. Numerical simulation of heat dissipation processes in underground power cable system situated in thermal backfill and buried in a multilayered soil. *Energy Conv. Manag.* **2015**, *95*, 352–370. [CrossRef]

23. *NTE 007/08/00*; Normative Document Regarding the Design and Execution of the Electrical Cable Networks. ANRE: Bucharest, Romania, 2008. Available online: https://anre.ro/wp-content/uploads/2023/04/ORDIN_38_NTE_007_Normativ.pdf (accessed on 20 April 2023). (In Romanian)
24. Fericean, S. *Inductive Sensors for Industrial Applications*, 1st ed.; Artech House: Norwood, NJ, USA, 2019.
25. *Maxwell Help*, Release 2021 R1; ANSYS, Inc.: Canonsburg, PA, USA, 2021.
26. *IEC 60287-1-1*; Electric Cables—Calculation of the Current Rating—Part 1-1: Current Rating Equations (100% Load Factor) and Calculation of Losses—General, Edition 2.1. International Electrotechnical Commission: Geneva, Switzerland, 2014.
27. Lunca, E.; Neagu, B.C.; Vornicu, S. Finite Element Analysis of Electromagnetic Fields Emitted by Overhead High-Voltage Power Lines. In *Numerical Methods for Energy Applications*, 1st ed.; Mahdavi Tabatabaei, N., Bizon, N., Eds.; Springer: Cham, Switzerland, 2021; Volume 1, pp. 795–821. [CrossRef]
28. International Commission on Non-Ionizing Radiation Protection. ICNIRP Guidelines for Limiting Exposure to Time-Varying Electric, Magnetic, and Electromagnetic Fields (up to 300 GHz). *Health Phys.* **1998**, *74*, 494–522.